Progress In Electromagnetics Research C, Vol. 136, 199–213, 2023

Uncertainty Quantification of Electromagnetic Exposure of Human Body with Medical Aortic Valve Stent Implants under an EV-WPT Device

Tianhao Wang[1], Bo Li[1], Quanyi Yu[1], Yangyun Wu[1], Linlin Xu[1], Yaodan Chi[2], and Baizhi Li[3, *]

Abstract—With the gradual popularization of high-power electric vehicle wireless power transfer (EV-WPT) applications, the safety issue of human exposure to electromagnetic fields leaked from EV-WPT devices has received considerable attention. In particular, careful attention should be devoted to human protection from electromagnetic field issues among people with medical implants. Considering the electromagnetic coupling between a human aortic valve metal stent (AVS) and the leakage field, this study establishes a numerical simulation model of the electromagnetic exposure of a human implanted with AVS to the leakage electromagnetic field of EV-WPT on the basis of human medical ethics. Given the existence of many uncertainties in actual WPT charging, which may cause damage to a human heart implanted with AVS, an orthogonal matching pursuit sparse generalized polynomial chaos expansion (OMP-sgPCE) method is developed to conduct an uncertainty quantification of the maximum induced electric field intensity ($E_{\max}$) of a human heart implanted with AVS. Results indicate that the induced $E_{\max}$ obtained by this method can exceed the ICNIRP guideline limit and may seriously endanger human heart safety. This study also adopts the Sobol method to obtain the degree of influence of the coil group's spatial location parameters and the AVS geometric parameters on the induced $E_{\max}$, thereby providing a reasonable theoretical basis and scientific guidance for the optimal design of EV-WPT devices and AVS.

1. INTRODUCTION

In the current society with the rapid development of science and technology, wireless power transfer (WPT) technology is widely used to charge various electronic devices, such as electric vehicles (EVs) [1], medical implants [2], and smartphones [3]. To achieve rapid charging of EVs, high-power and high-frequency WPT devices need to be developed [4, 5]. Studying the electromagnetic exposure potential adverse health effect posed by high-power EV-WPT devices on human bodies is essential [6, 7]. With regard to the protection of humans from electromagnetic fields of EV-WPT devices, studies have been conducted on the leakage magnetic field of EV-WPT [8], the electromagnetic induction amount in the human voxel model [9], and electromagnetic protection for the human body [10]. The safety of humans with medical implants from electromagnetic exposure should be considered, especially when these humans are exposed to high-intensity electromagnetic fields generated by these high-power WPT devices.

To ensure safe human electromagnetic exposure, the leakage electromagnetic field generated by WPT devices must comply with relevant international standards. The International Commission on

Received 7 June 2023, Accepted 9 August 2023, Scheduled 20 August 2023

* Corresponding author: Baizhi Li (libaizhi@jlu.edu.cn).

[1] The College of Instrumentation and Electrical Engineering, Jilin University, Changchun 130026, China. [2] Jilin Provincial Key Laboratory of Architectural Electricity and Comprehensive Energy Saving, Jilin Jianzhu University, Changchun 130118, China. [3] The College of Pharmaceutical Sciences, Jilin University, Changchun 130021, China.

Non-Ionizing Radiation Protection (ICNIRP) and the Institute of Electrical and Electronics Engineers provide indicators of concern at different frequencies. When the frequency is lower than 100 kHz, the intensity of induced electric field strength (E) becomes the main concern to avoid the stimulation of nerve tissue. When the frequency is higher than 100 kHz, the specific absorption rate (SAR) value should be the main concern to prevent the human body's core temperature from rising [11, 12]. The heart is the most important organ in the human body, and aortic valve stenosis is often accompanied by coronary artery disease, leading to myocardial infarction [13]. Metal aortic valve stents (AVSs) are usually used to permanently implant stenotic valves for achieving normal blood delivery by the heart [14]. [15] showed when the human body is exposed to electromagnetic fields generated by magnetic resonance imaging, heart implants may absorb electromagnetic radiation energy and generate heat, which can cause damage to nearby heart tissues. Therefore, the influence of the electromagnetic field leakage of an EV-WPT device on a human heart implanted with AVS must be considered.

The electromagnetic exposure of humans with metal implants near a WPT device has been studied. [16] discussed the induced E of human tissues adjacent to implants under EV-WPT electromagnetic leakage of 85 kHz. The local temperature rise of tissues around human metal implants under a radio frequency field was studied in [17]. The study evaluated the impact of head bone plate implants on SAR in a head model under WPT with a power of 50 W and a frequency of 6.78 MHz [18]. [19] calculated and evaluated the human protection from electromagnetic fields of the leakage electromagnetic field of WPT with a frequency of 1470 MHz in capsule and skin implants. Notably, only a few studies have been conducted on the protection from electromagnetic fields of human hearts implanted with AVS under the leakage electromagnetic field of EV-WPT despite the importance of cardiac organs and the widespread use of AVS in the treatment of aortic stenosis. Moreover, the electromagnetic field values near the sharp edges and tips of metal implants located under an electromagnetic field are large [16, 17], which may cause damage to human heart tissues implanted with AVS. At the same time, due to the different installation environments of EV-WPT devices and the manufacturing process of AVS, the coil group's spatial location parameters and the AVS geometric parameters are uncertain, which causes a human heart implanted with AVS to produce an electromagnetic field with an uncertain distribution. Uncertainty quantification of the electromagnetic exposure of human metal AVS implants in EV-WPT devices is important.

At present, research on the uncertainty quantification of human electromagnetic exposure to EV-WPT-containing medical implants has not been conducted. Many, uncertainty quantification methods, such as deep learning [20], partial least squares regression [21], and adaptive sparse polynomial chaos expansion (PCE) [22], have been applied to optimize the transmission efficiency design of EV-WPT devices. The research on the uncertainty quantification of human electromagnetic exposure mainly includes the use of optimized random greedy PCE in the uncertainty quantification of the electromagnetic exposure indicators of the human body and multiple organs under different exposure scenarios [23]. In [24], a combination of the PCE method and global sensitivity was employed to study human head SAR under electromagnetic radiation from a mobile phone. However, the traditional PCE method leads to a high calculation cost due to problems in calculating the "curse of dimensionality." Therefore, in this study, the orthogonal matching pursuit sparse generalized PCE (OMP-sgPCE) method is proposed to achieve an efficient uncertainty quantification of the electromagnetic exposure of a human with a medical implant. Based on this, the Sobol global sensitivity analysis method is used to quantify the influence of uncertain factors to understand the impact of the EV-WPT devices on the electromagnetic exposure of a humans with a medical implant and to further provide scientific guidance for the optimal design of EV-WPT devices or medical implants. Based on the idea of variance decomposition, [25] proposed to calculate the global sensitivity index of the model combination with the Monte Carlo (MC) method and named it the Sobol global sensitivity analysis method. In [26], the Sobol global sensitivity analysis method was combined with the gPCE method, which greatly improves the computational efficiency of calculating the global sensitivity index of the mathematical model due to the unfolded form of the gPCE method. And it has been successfully applied in the fields of human immunomedicine [27], safety assessment of groundwater [28], and electromagnetic compatibility of printed circuit boards [29].

In this paper, a safety assessment model of the electromagnetic exposure of an adult implanted with AVS is established to address the leakage electromagnetic field of an EV-WPT device with a

power of 22 kW and a frequency of 85 kHz. Considering that the human body is located in the position nearest to the electromagnetic exposure center of EV-WPT, the OMP-sgPCE method is proposed to realize the uncertainty quantification of the electromagnetic exposure of a human heart implanted with AVS. The Sobol method is also adopted to achieve a global sensitivity analysis of relevant influencing factors and to provide a reasonable theoretical basis and scientific guidance. The rest of this paper is organized as follows. In Section 2, an electromagnetic numerical simulation model of an AVS-implanted human heart is established based on the leakage electromagnetic field scenario of an EV-WPT device. Section 3 introduces the uncertainty quantification framework of the electromagnetic exposure of the AVS-implanted human heart. Section 4 discusses the results of the uncertainty quantification and global sensitivity analysis of induced $E_{\max}$ by the human heart implanted with AVS. Section 5 summarizes this paper.

2. NUMERICAL SIMULATION MODEL

2.1. Electromagnetic Numerical Simulation Model of EV-WPT

To calculate the EV-WPT electromagnetic field, an electromagnetic numerical simulation model of EV-WPT is established using the professional electromagnetic simulation software of the finite element method. Fig. 1 shows the EV-WPT device and the human body models proposed in this study. The size of the EV model is $4000 \times 2000 \times 1500$ mm (length $\times$ width $\times$ height). The geometric shape of the EV is accurately considered, and it is basically consistent with the size in common cars. The spatial location parameters of the coil's group are shown in Fig. 1(d), and the geometric parameters of the coil's group are shown in Fig. 2. The size of the transmitting coil, T_X, of the WPT device, is similar to that of the receiving coil, R_X. The outer and inner dimensions are 600×600 and 300×300 mm, respectively. The number of coil turns is 11, the coil sectional area s_0 is 3 mm^2, and the outer dimension of the shielding layer is $600 \times 600 \times 10$ mm (length $\times$ width $\times$ thickness). Considering the actual usage scenario, the initial distance y_0 between T_X and R_X is set to 200 mm, and the initial lateral offset z_0 and longitudinal offset x_0 are set to 0 mm. In consideration of the closest position between human electromagnetic exposure and the WPT device in practical applications, the human body is placed on the side of the EV 900 mm from the WPT device's electromagnetic exposure center. The equivalent circuit diagram of the WPT device is shown in Fig. 3, and the compensation circuit of the WPT device adopts a series-series (SS)

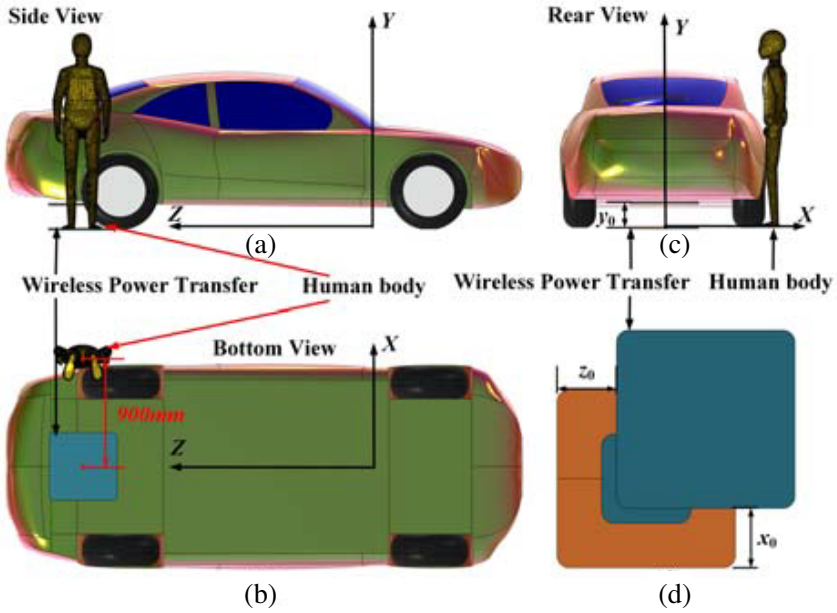

Figure 1. Relative position of the vehicle in the EV-WPT device scenario: (a) side view, (b) bottom view, (c) rear view, and (d) dislocation between the transmitting and receiving ends of the WPT device.

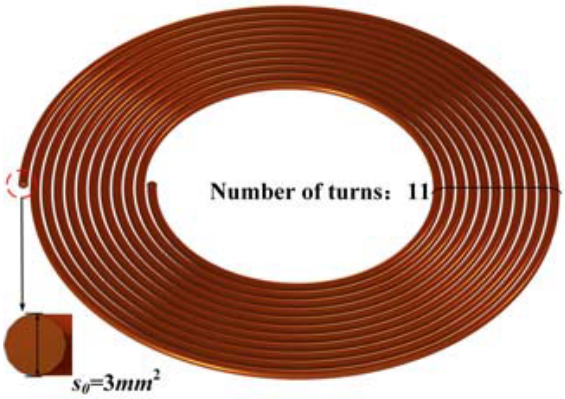

Figure 2. WPT coil geometry model diagram.

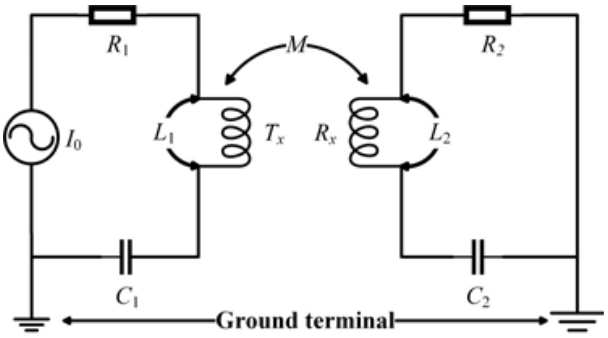

Figure 3. Equivalent schematic diagram of WPT device circuit.

connection type compensation circuit. Among them, I_0 is the constant current excitation source, R_1 is the sum of the internal resistance of the excitation source and T_X, with a value of 0.21 Ω. C_1 and C_2 are the compensation capacitors of T_X and R_X, with values of 126.6 nF and 126.8 nF, respectively. R_2 is the sum of the internal resistance of the load and R_X, with a value of 10.23 Ω. L_1 and L_2 are the self-inductance of T_X and R_X, with values of 1.16 mH and 1.13 mH, respectively. M is the mutual inductance of T_X and R_X. In this way, the modeling of the EV-WPT electromagnetic simulation numerical model is completed.

2.2. Numerical Model of the Human Body and AVS

This study reconstructs the human body and organ model on the basis of real scanned human CT data, as shown in Fig. 4. The model considers the combination of the human body and the heart. The height

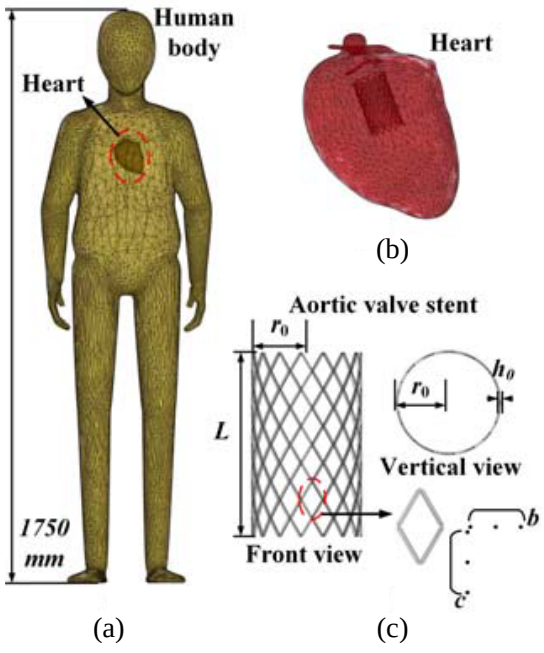

Figure 4. AVS-implanted heart human body model, (a) human heart organ joint model, (b) heart model, and (c) medical AVS geometric model.

and weight of the human body are 1750 mm and 75 kg, respectively. Considering that the conductivity and relative dielectric constant of the human body at 85 kHz are 0.27 S/m and 5400, respectively, the conductivity and relative dielectric constant of the heart are set to 0.21 S/m and 11,137, respectively. In this paper, AVS geometric structure refers to that in [30], the arrangement along the circumference of bracket b is 15, and the arrangement along the axial direction of bracket c is 5. In accordance with the actual patient's aortic structure, the axial length L of the metal bracket is 33.5 mm, the initial stent radius r_0 is 10 mm, and the wall thickness h_0 is 0.4 mm. Titanium alloy has the best characteristics, such as corrosion resistance, biocompatibility, fatigue resistance, toughness, and memory, required by implant materials. It is widely used in orthopedic, cardiovascular, and other biomedical equipment. Therefore, the AVS implant material considered in this study is a nickel-titanium alloy with a uniform texture, and its conductivity and relative dielectric constant are respectively set to 2.38×10^6 S/m and 1 [16]. When AVS made of nickel-titanium alloy is implanted into the heart and exposed to the electromagnetic environment generated by an EV-WPT device, it may cause an uneven distribution of induced E in the cardiac tissue on the surface of AVS, thereby seriously affecting the normal physiological function of the heart.

2.3. Numerical Simulation Calculation Method

In electromagnetic field analysis, when the wavelength of electromagnetic waves in space is larger than the size of the target to be solved, the magnetic quasi-static (MQS) method is used to calculate electromagnetic parameters. The approximate conditions for the MQS method are:

$$\kappa^2 Z^2 \ll 1 \tag{1}$$

$$\kappa^2 = \omega(\omega\varepsilon + j\sigma)\mu_0 \tag{2}$$

where κ is the wave number in the space medium. In the case of no loss, the relationship between κ and wavelength λ is $\kappa = 2\pi/\lambda$; ω is the angular frequency of the electromagnetic field; ε and σ are the dielectric constant and conductivity of the human tissue; μ is the permeability of $4\pi \times 10^{-7}$ (H/m); and Z is the diameter of the calculation area.

In the numerical simulation of human electromagnetic exposure at a frequency of 85 kHz, the free space wavelength is on the order of tens of meters, and the electromagnetic indicators inside the human body and organ tissues are calculated using the MQS method [31]. The MQS method is divided into two steps. Firstly, the spatial distribution of the leakage electromagnetic field generated by the EV-WPT device is calculated using a multi-physical field finite element simulation software to obtain the magnetic vector. Then, the electromagnetic indicators inside the human body are solved based on the relationship between the magnetic vector and Maxwell's equations.

When the leakage electromagnetic field generated by EV-WPT devices with a frequency less than 100 kHz has adverse effects on the human body, the ICNIRP [2010] guideline limit is the induced E inside the human body [32]. According to ICNIRP recommendation, the vector average of induced E in a continuous volume of $2 \times 2 \times 2\,\text{mm}^3$ is used to evaluate induced E in the human body. This paper uses a mesh size of $1.5 \times 1.5 \times 1.5\,\text{mm}^3$ is used to partition the human body model, which meets the continuous tissue volume requirements for estimating the induced E of the human body in accordance with the ICNIRP guidelines [32, 33]. Considering the geometric precision of the AVS model, a lower grid resolution will not yield accurate numerical results. Therefore, this paper adopts a grid size of $0.2 \times 0.2 \times 0.2\,\text{mm}^3$ is used to divide it, and due to the disadvantage of using the 99th percentile method to calculation-uniform human body mentioned in ICNIRP [2020], this paper uses the actual value of induced E around the implant for numerical calculation and analysis.

This paper uses professional multi-physical field commercial software to solve the electromagnetic exposure index of an EV-WPT device with a power of 22 kW and a frequency of 85 kHz implanted with AVS using the MQS method, in order to achieve the calculation of the electromagnetic numerical simulation model. Considering the call of relevant variables in the numerical model and uncertainty quantification work, the uncertainty quantification work of the above numerical model is achieved through the commercial mathematical software MATLAB.

3. UNCERTAINTY QUANTIFICATION METHODS AND GLOBAL SENSITIVITY ANALYSIS OF ELECTROMAGNETIC EXPOSURE OF THE HUMAN HEART IMPLANTED WITH AVS UNDER AN EV-WPT DEVICE

3.1. Theory of sgPCE

Xiu and Karniadakis proposed the Askey scheme to extend Wiener PCE to gPCE [34], which is widely used to solve the uncertainty quantification problem in the engineering field. The original model of the electromagnetic exposure of the human heart implanted with AVS is infinitely expanded by multidimensional orthogonal polynomials as follows:

$$\begin{aligned} y(\xi) &= c_0 I_0 + \sum_{a_1=1}^{\infty} c_{a_1} I_1(\xi_{a_1}) + \sum_{a_1=1}^{\infty}\sum_{a2=1}^{a_1} c_{a_1 a_2} I_2(\xi_{a_1},\xi_{a_2}) + \sum_{a_1=1}^{\infty}\sum_{a_2=1}^{a_2}\sum_{a_3=1}^{a_1} c_{a_1 a_2 a_3} I_3(\xi_{a_1},\xi_{a_2},\xi_{a_3}) + ... \\ &= \sum_{a\in\Re_0^d} c_\alpha \Phi_\alpha(\xi), \end{aligned} \tag{3}$$

$$\alpha \in \Re_0^d = \{(a_1, a_2, ..., a_d) : a_j \in \Re \cup \{0\}\}, \tag{4}$$

where d is the input variable dimension; $c_\alpha = c_{a_1 a_2 ... a_n}$ refers to the polynomial coefficients; $\Phi_\alpha(\xi)$ is $I_n(\xi_{a_1}, \xi_{a_2}, ..., \xi_{a_n})$; and $I_n(\xi_{a_1}, \xi_{a_2}, ..., \xi_{a_n})$ is an n-order mixed orthogonal polynomial function with respect to ξ.

Considering that the infinite expansion of the electromagnetic exposure gPCE of the human heart implanted with AVS caused by an EV-WPT device cannot be calculated, on the premise of achieving calculation accuracy, (4) can be reasonably truncated as follows:

$$y^p(\xi) = \sum_{\alpha=0}^{p} c_\alpha \Phi_\alpha(\xi), \tag{5}$$

where p is the truncation order. The number of expanded items after gPCE truncation is expressed as follows:

$$P = \frac{(p+d)!}{p!d!}. \tag{6}$$

The conventional gPCE method uses the ordinal least squares (OLS) method to obtain the coefficients by substituting the sample $\xi^S = [\xi_1^S, ..., \xi_j^S, ..., \xi_N^S]^T$ and the corresponding functional response value $G = [g(X_1^S), ..., g(X_N^S)]^T$ of electromagnetic exposure into the ends of (5) of the gPCE model.

$$\underbrace{\begin{bmatrix} \Phi_0(\xi_1^S) & \Phi_1(\xi_1^S) & ... & \Phi_P(\xi_1^S) \\ \Phi_0(\xi_2^S) & \Phi_1(\xi_2^S) & ... & \Phi_P(\xi_2^S) \\ ... & ... & & ... \\ \Phi_0(\xi_N^S) & \Phi_1(\xi_N^S) & ... & \Phi_P(\xi_N^S) \end{bmatrix}}_{A} \underbrace{\begin{bmatrix} b_0 \\ b_1 \\ ... \\ b_P \end{bmatrix}}_{b} = \underbrace{\begin{bmatrix} g(X_1^S) \\ g(X_2^S) \\ ... \\ g(X_N^S) \end{bmatrix}}_{G}. \tag{7}$$

(7) can be abbreviated as $Ab = G$, and (8) uses linear OLS to calculate gPCE coefficients.

$$J(b) = \sum_{j=1}^{N} \varepsilon_j^2 = \sum_{j=1}^{N} \left[g(X_j^S) - \hat{g}(\xi_j^S)\right]^2, \tag{8}$$

$$\hat{g}(\xi_j^S) = \sum_{i=1}^{P} b_i \Phi_i(\xi_j^S). \tag{9}$$

In (8) and (9), $\hat{g}(\xi_j^S)$ is the response value of the electromagnetic exposure function estimated at each sample point on the basis of the gPCE model. In accordance with OLS, the gPCE coefficients, (10) can be obtained with (8) as follows:

$$b = (AA^T)^{-1} A^T G. \tag{10}$$

Given that the coefficients of gPCE calculated by the OLS method are not sparsely processed, and in consideration of multi-dimension and diversity, uncertainty quantification of electromagnetic exposure through multi-dimensional finite element numerical calculation is considered. The uncertainty quantification program is written using MATLAB in this study, and when using EV-WPT to calculate the 3D simulation model of the electromagnetic exposure of the human heart implanted with AVS, the computational efficiency is seriously affected. Therefore, this study uses the OMP sparse algorithm to calculate the coefficients of gPCE. The OMP method is a greedy algorithm that adopts the principle of iteration. Compared with the OLS method, it can accurately build the output of the model when the number of sample points is small. The calculation process of the OMP method is a cyclic iterative process, which minimizes the approximate residual of each iteration. Consider the approximate residuals $\mathbf{m}_k$ for polynomial bases of k elements and $\mathbf{m}_{k+1}$ for polynomial bases of $k+1$ elements $\mathbf{m}_{k+1}$. Project the residual $\mathbf{m}_k$ onto a new polynomial to obtain:

$$\mathbf{m}_k = \langle \mathbf{m}_k, \Psi_{k+1} \rangle \Psi_{k+1} + \mathbf{m}_{k+1}. \tag{11}$$

At the t^{th} iteration, OMP finds the most relevant basis function $\boldsymbol{\beta}_k^{(t-1)}$ with residual $\mathbf{m}^{(t-1)}$ in the candidate set $A^{(t-1)}$. And add it to the activity set $k \in A^{(t-1)}$. The iterative process of OMP can be expressed as (12).

$$i^{(t)} = \arg\max_{k \in A^{(t-1)}} \left| \left\langle \mathbf{m}^{(t-1)}, \beta_k \right\rangle \right|. \tag{12}$$

The polynomial coefficients of gPCE calculated through the OLS method from the t^{th} iteration are $\mathbf{c}^{(t-1)}$. At this point, the training residuals $\mathbf{m}^{(t-1)}$ used in (12) can be determined through $\mathbf{m}^{(t-1)} = \beta^{(t-1)}\mathbf{c}^{(t-1)} - \mathbf{y}$. After choosing the base function, the new coefficients of gPCE can be calculated through OLS. The above steps are repeated until the norm of the residual meets the requirements; its pseudocode is shown in Table 1.

Table 1. Pseudo code for calculating PCE coefficients by the OMP-sgPCE method.

Algorithm 1: Orthogonal Marching Pursuit

Input: Candidate set A of basis function $\{\boldsymbol{\beta}_i\}_{i=1}^{P}$, Matlab input sampling points of input variables $\{\xi_i\}_{k=1}^{N}$, Electromagnetic numerical simulation model corresponding output $\mathbf{y} = \{y(\boldsymbol{\xi}_k)\}_{k=1}^{N}$

Output: Index Υ of the chosen basis function, polynomialcoefficients $\mathbf{c}$ of gPCE

1 Iteration $t \leftarrow 0$, $\Upsilon^{(0)} \leftarrow \varnothing$, $A^{(0)} \leftarrow A$, $\mathbf{m}^{(0)} \leftarrow \mathbf{y}$

2 Set cross-validation error δ

3 **While** $\left\|\mathbf{m}^{(t)}\right\|_2 > \delta$ **do**

4 $t = t+1$

5 Choose the most relevant basis function $\boldsymbol{\beta}_k^{(t-1)}$ with residual $\mathbf{m}^{(t-1)}$ in the candidate set $A^{(t-1)}$ by (12)

6 Merge $i^{(t-1)}$ into the activity set: $\Upsilon^{(t)} = \Upsilon^{(t-1)} \cup i^{(t)}$

7 Remove the part of the candidate set that intersects with X: $A^{(t)} \leftarrow A^{(t-1)} - A^{(t-1)} \cap i^{(t)}$

8 Solve the coefficients ofgPCE at this pointthrough the OLS method: $\Psi^{(t)}\mathbf{c}^{(t)} = \mathbf{y}$,where $\Psi^{(t)}$ obtain $\boldsymbol{\beta}_i$, $i \in \Upsilon^{(t)}$

9 Recalculate residual: $\mathbf{m}^{(t-1)} = \boldsymbol{\beta}^{(t-1)}\mathbf{c}^{(t-1)} - \mathbf{y}$

10 **Endwhile**

By solving coefficients of gPCE and substituting them (5), the OMP-sgPCE proxy model of electromagnetic exposure to an EV-WPT device with multidimensional random input variables to the human heart implanted with AVS is obtained. Then, in accordance with the distribution type

and input random variable dimension, probability density function (PDF) $f_Y(y)$ is derived. From $F_Y(y) = F(f_Y(y))$, the probability density distribution function is obtained, and the mean value, variance, and probability of exceeding the limit of the model are calculated in accordance with the gPCE coefficients obtained from (13).

$$\begin{cases} \text{mean} = \hat{c}_0 \\ \text{var} = \sum_{i=1}^{p} \left[c_i^2 \left\langle \Phi_i^2 \right\rangle \right] \\ \text{probability} = \int_{\text{limit}}^{+\infty} f_y(y) dy \end{cases}. \tag{13}$$

3.2. Sobol Global Sensitivity Analysis

Analyzing the influence of the multidimensional random input variables of the EV-WPT device on the electromagnetic exposure of the human heart implanted with AVS can provide a theoretical basis for the optimization of human body protection. The OMP-sgPCE method introduced in the previous section is combined with the Sobol method to achieve efficient calculation of the global sensitivity index. The global sensitivity analysis uses the principle of variance decomposition to express the original model as the Sobol sensitivity index, and the first-order sensitivity is expressed as follows:

$$S_{X_i} = \frac{V_{X_i}\left(E_{X_{-i}}\left(Y|x_i\right)\right)}{V\left(Y\right)}. \tag{14}$$

The formula above shows the influence of the multidimensional random input variable X_i on the electromagnetic exposure model of the human heart implanted with AVS. The size of S_{X_i} is proportional to the importance of the variable X_i. The larger S_{X_i} is, the greater the influence of X_i is. For the molecule $V_{X_i}(E_{X_{-i}}(Y|x_i))$ in the formula above, its relative $V_{X_{-i}}(E_{X_{-i}}(Y|x_{-i}))$ represents the influence of parameters other than X_i on the model. $V(Y) - V_{X_{-i}}(E_{X_{-i}}(Y|x_{-x}))$ represents the influence extent of all items related to X_i on Y, and the total effect sensitivity of X_i can be expressed as

$$S_{X_i}^T = \frac{V\left(Y\right) - V_{X_{-i}}\left(E_{X_{-i}}\left(Y|x_{-i}\right)\right)}{V\left(Y\right)}. \tag{15}$$

The process of calculating the global sensitivity index of multidimensional random input variables in combination with the MC method is as follows. First, two sets of sample matrices A_{Nn} and B_{Nn} of X are generated in accordance with the distribution of the input variables. Each row in the matrix corresponds to samples of different input variables, and N is the number of samples.

Replacing the i^{th} column of matrix A_{Nn} with the i^{th} column of matrix B_{Nn} yields a new matrix C_{Ni} as follows:

$$C_{Nni} = \begin{bmatrix} x_{11} & x_{12} & \cdots & x'_{1i} & \cdots & x_{1n} \\ x_{21} & x_{22} & \cdots & x'_{2i} & \cdots & x_{2n} \\ \vdots & \vdots & \vdots & \vdots & \vdots & \vdots \\ x_{N1} & x_{N1} & \cdots & x'_{Ni} & \cdots & x_{Nn} \end{bmatrix}. \tag{16}$$

The response values of matrix A_{Nn}, B_{Nn}, and C_{Ni} can be calculated with the model $g(X)$ as follows:

$$y_A = g\left(A\right), \ y_B = g\left(B\right), \ y_C = g\left(C\right). \tag{17}$$

From the derivation above, the total sensitivity index and first-order sensitivity index of random input variables X_i of the MC method model can be obtained as

$$S_{Ti} = 1 - \frac{(1/N)\sum_{j=1}^{N} y_A^j y_{C_i}^j - g_0^2}{(1/N)\sum_{j=1}^{N} \left(y_A^j\right)^2 - g_0^2}, \tag{18}$$

$$S_i = \frac{(1/N)\sum_{j=1}^{N} y_A^j y_{C_i}^j - g_0^2}{(1/N)\sum_{j=1}^{N} \left(y_A^j\right)^2 - g_0^2}. \tag{19}$$

Combined with the coefficients of OMP-sgPCE, the global sensitivity index of different random input variables can also be obtained effectively. The first-order sensitivity index of X_i in (14) can be expressed as follows:

$$S_{X_i} = \frac{Var\left[E\left(Y|\xi_i\right)\right]}{Var\left(Y\right)} = \frac{\sum_{i\in I_i} c_i^2 E\left(\varphi_i^2\right)}{\sum_{i=1}^{m-1} c_i^2 E\left(\varphi_i^2\right)}, \tag{20}$$

where ξ_i represents the standard normal random variable corresponding to x_i; I_i represents the set of polynomial φ_i containing random variable ξ_i; and c_i represents the coefficient of polynomial φ_i.

Combined with the coefficients of OMP-sgPCE, the total sensitivity index of input parameter X_i is expressed as

$$S_{X_i}^T = 1 - S_{X_i}. \tag{21}$$

The global sensitivity index of the OMP-sgPCE proxy model with multidimensional input variables can be obtained from (20) and (21). In this study, the correlation framework of the uncertainty quantification of the electromagnetic exposure of the human heart implanted with AVS and the global sensitivity analysis is shown in Fig. 5.

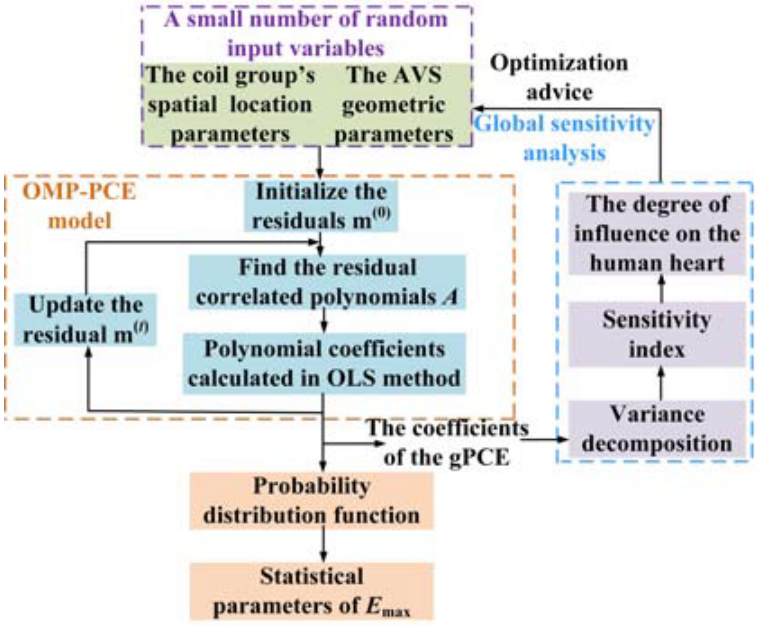

Figure 5. Association framework of uncertainty quantification and Sobol global sensitivity analysis.

4. NUMERICAL SIMULATION RESULTS AND DISCUSSION

In this study, an electromagnetism simulation model of the human heart implanted with AVS is established under an electromagnetic exposure scenario from an EV-WPT device with a power of 22 kW and frequency of 85 kHz. The initial parameters for the coil group's spatial location parameters

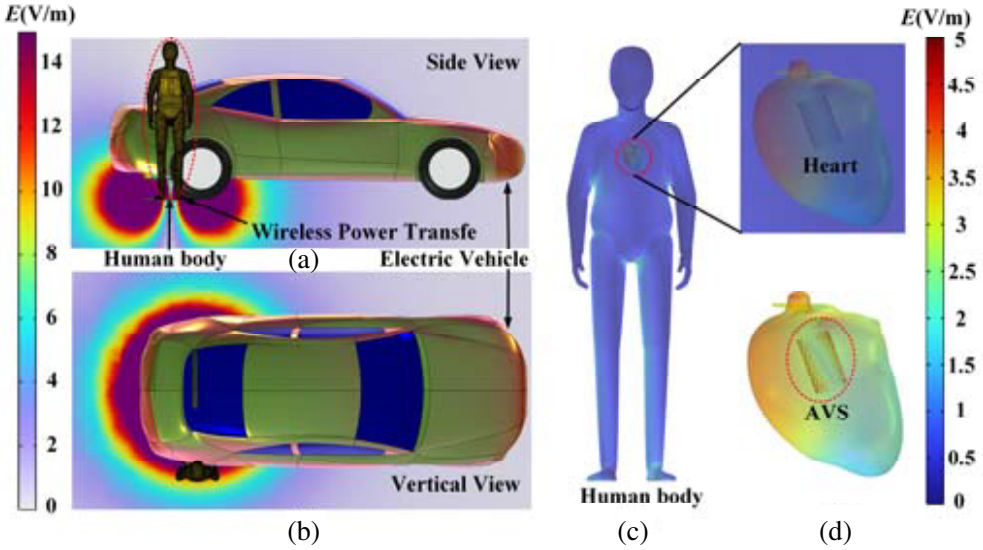

Figure 6. Induced E distribution of the human body implanted with AVS under the electromagnetic exposure scenario of the EV-WPT device: (a) side view angle of induced E distribution spatial distribution, (b) vertical view angle of induced E distribution spatial distribution, (c) induced E distribution of the human body, and (d) enlarged view of induced E distribution of the heart.

Table 2. Distribution type of random input variable.

Random variables	Distributed parameters	Unit
variation of coil group's distance y	$U(-100, 100)$	mm
coil group's longitudinal offset value z	$U(-200, 200)$	mm
coil group's lateral offset value x	$U(-200, 200)$	mm
the radius value of AVS r	$N(10, 1/3)$	mm
the wall thickness value of AVS h	$N(4 \times 10^{-1}, 4 \times 10^{-2}/3)$	mm

and the AVS implant geometric parameters introduced in Section 2 are set as follows: $y_0 = 200\,\text{mm}$, $z_0 = 0\,\text{mm}$, $x_0 = 0\,\text{mm}$, $r_0 = 10\,\text{mm}$, and $h_0 = 0.4\,\text{mm}$. The distribution diagram results of induced E from different perspectives are shown in Figs. 6(a) and 6(b), and the distribution diagram results of induced E for the human heart implanted with AVS are shown in Figs. 6(c), and 6(d). According to low-frequency ICNIRP guidelines, when the operating frequency of an EV-WPT device is 85 kHz, the induced E limit of the human body is $11.475\,\text{V/m}$. Figs. 6(c) and 6(d) show that the large value of induced E is distributed near AVS, and the induced $E_{\max}$ of the heart under the condition of the initial parameters is $6.1457\,\text{V/m}$. Considering the differences in driver operation, installation environment, and AVS's manufacturing process, the variation of the coil group's distance y, the value of the coil group's longitudinal offset z, the value of the coil group's lateral offset value x, the value of the AVS's radius value r, and the value of wall thickness h exhibit uncertainty. The induced $E_{\max}$ of the heart is also uncertain, which may have a great impact on human protection from electromagnetic fields problems of the human body. In combination with the actual application scenario of the EV-WPT device, the coil group's spatial location parameters y, z, and x are set to be evenly distributed, and AVS geometric parameters r and h are set to have a normal distribution. At the same time, the geometric parameter error is considered to be $\pm 10\%$. The detailed parameters are shown in Table 2. In this study, a personal computer is used for the numerical simulation calculation. The CPU model is i9-13900K, with 24 cores and 32 threads, Rui frequency of 5.8 GHz, memory of $32\,\text{GB} \times 4$, and frequency of 3200 MHz.

To verify the accuracy and efficiency of the OMP-sgPCE method, this study compares the classic

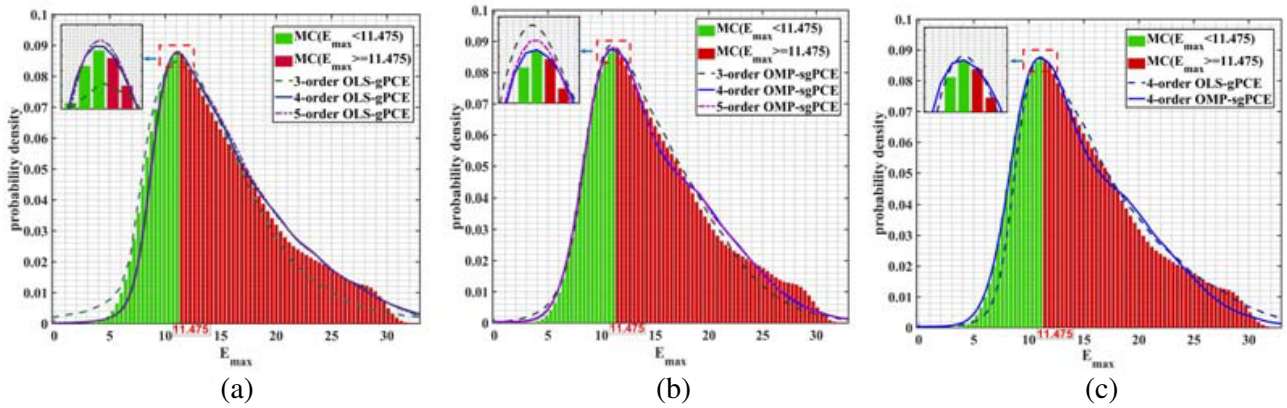

Figure 7. PDF curve of $E_{\max}$ induced by the human heart implanted with AVS with the EV-WPT device: (a) comparison of PDF curves calculated by the MC method and OLS-gPCE method with different truncation orders, (b) comparison of PDF curves calculated by the MC method and OMP-sgPCE method with different truncation orders, and (c) comparison of PDF curves calculated by the 4-order OMP-sgPCE method and OLS-sgPCE method.

Table 3. Sample points required by MC, OMP-sgPCE, and OLS-sgPCE methods with different truncation orders, calculated results of relevant parameters, and calculation time.

Different methods and truncation order	Mean value of $E_{\max}$ (V/m)	Variance of $E_{\max}$ (V^2/m^2)	Probability of transfinite	Sample point	Time (min)
3-order OLS-gPCE	15.654	35.146	0.725	120	3190
3-order OMP-sgPCE	14.478	27.666	0.675	51	1356
4-order OLS-gPCE	14.604	43.419	0.673	180	4758
4-order OMP-sgPCE	14.784	30.594	0.678	63	1675
5-order OLS-gPCE	14.773	45.317	0.671	700	18609
5-order OMP-sgPCE	14.876	31.482	0.676	101	2685
MC	14.947	29.380	0.684	10000	265868

MC method and the traditional OLS-gPCE method. Next, a test based on the relevant random input variables set in Table 2 is conducted. The calculation of the statistical parameters of the induced $E_{\max}$ in the human heart implanted with AVS confirms that the results of the MC method adopting 10,000 sample points are stable. Therefore, 10,000 sample points are selected for the MC method in the comparison, and the three methods are used for the uncertainty quantification of the induced $E_{\max}$ of the human heart implanted with AVS under the EV-WPT electromagnetic exposure scenario. The comparison of the PDF curve calculation results of the different methods is shown in Fig. 7. The sample points required by the relevant uncertainty quantification algorithm and the calculated statistical characteristic parameters of induced $E_{\max}$ are shown in Table 3. As indicated in Figs. 7(a) and (b), the fitting effects of the OMP-sgPCE and OLS-gPCE methods using truncation orders of 3, 4, and 5 are evaluated and compared with the PDF curve of the MC method. As shown in Fig. 7(c), the fitting effects of the OMP-sgPCE and OLS-gPCE methods with truncation orders of 4 and the MC method calculated PDF curves are evaluated. The following conclusions are drawn from the comparison. The OMP-sgPCE and OLS-gPCE methods with truncation orders of 4 and 5 and the MC method have similar fitting effects on the PDF curves, and all of the results are better than those of the PDF curves calculated with truncation orders of 3.

According to the data in Table 3, the average value of induced $E_{\max}$ calculated by the different

methods exceeds the ICNIRP guideline's safety limit at a frequency of 85 kHz. Considering the number of sample points, calculation time, probability of exceeding the limit, mean value, and variance of $E_{\max}$, the variance value of the OMP-sgPCE method is similar to that of the MC method and is relatively low. The simulation dispersion degree of OMP-sgPCE is close, and the data stability is good. As shown in Fig. 7(c) and Table 3, in consideration of the statistical parameters and fitting effects, the 4-order OMP-sgPCE method ensures a PDF fitting effect that is close to that of the MC method while improving the computational efficiency by approximately 2.84 and 158.73 times compared with the OLS-gPCE method with the same truncation order and the MC method, respectively. In summary, in the numerical simulation experiment, the OMP-sgPCE method proposed in this study can achieve an efficient and high-precision uncertainty quantification of the electromagnetic exposure of the human heart implanted with AVS under the electromagnetic exposure scenario of the EV-WPT device.

The average value of the human heart's induced $E_{\max}$ obtained from the random variable distribution parameters in Table 2 exceeds 14.4 V/m, indicating that the average level exceeds the safety limit and that the probability of exceeding the limit is not less than 67%, which may pose a considerable threat to human safety. To evaluate the impact of 5D random input variables on the $E_{\max}$ of the human heart implanted with AVS under the EV-WPT device, this study also analyzes the global sensitivity of the induced $E_{\max}$ of the human heart implanted with AVS by using the MC method and the 4-order OMP-sgPCE method combined with the Sobol global sensitivity analysis method. The results are shown in Fig. 8.

As shown in Fig. 8, when the induced $E_{\max}$ of the human heart implanted with AVS is used as the output variable, the calculation results of the Sobol global sensitivity indicators of the 4-order OMP-sgPCE method and the MC method are similar, and the impact degree of the input variables is basically the same, verifying the accuracy of the 4-order OMP-sgPCE method combined with the Sobol method for global sensitivity analysis. Fig. 8 shows that the Sobol sensitivity index of the coil group's lateral offset value z is much greater than that of other variables, followed by the coil group's lateral offset value x, distance value y, and AVS' radius value r. AVS' thickness value h has the least impact on $E_{\max}$. Therefore, to ensure the electromagnetic exposure safety of the human heart implanted with AVS under the electromagnetic exposure scenario of an EV-WPT device with a power of 22 kW and frequency of 85 kHz, focused attention should be paid to ensuring that z is within a reasonable range in practical application scenarios while ensuring that the coil group offset value of the WPT device is also within a reasonable range. Further research should also be conducted on AVS structural design.

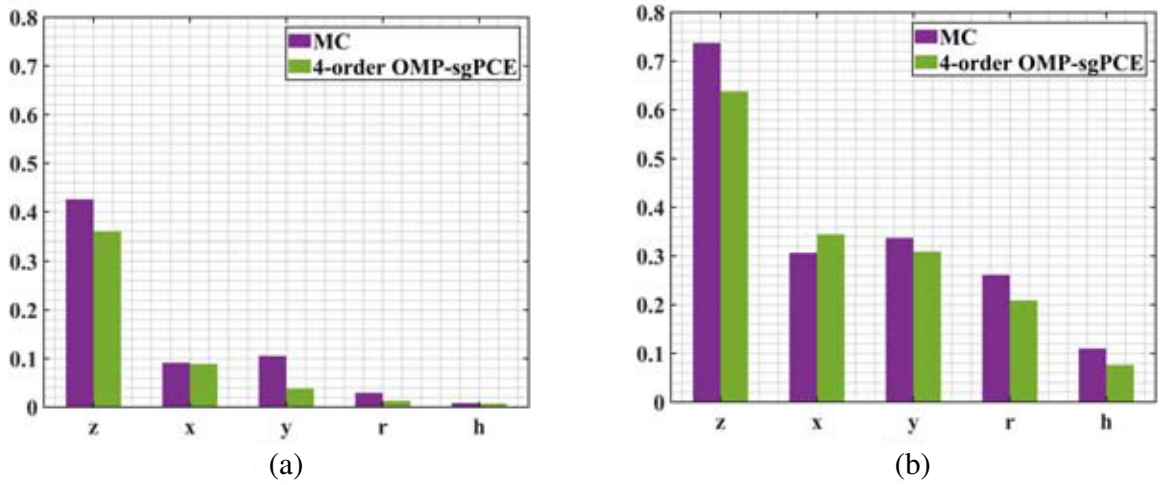

Figure 8. Induced $E_{\max}$ global sensitivity index of the human heart implanted with AVS under the EV-WPT device based on the 4-order OMP-sgPCE and MC methods: (a) first-order sensitivity and (b) total sensitivity.

5. CONCLUSION

The OMP-sgPCE method is used for uncertainty quantification of the induced $E_{\max}$ of AVS implants in cardiac tissue under electromagnetic exposure from an EV-WPT device. We consider the random uncertainty factors in real situations, study the closest exposure position of the human body to the EV-WPT device, and obtain the PDF curve and related statistical characteristic parameters that induce $E_{\max}$. Compared with the computational efficiency of the OLS-gPCE and MC methods, the computational efficiency of the 4-order OMP-sgPCE method increases by 2.84 and 158.73 times, respectively, while ensuring accuracy. The calculation results show that the induced $E_{\max}$ is distributed in the heart tissue near AVS, and the value of the induced $E_{\max}$ may exceed the ICNIRP guideline limit. The probability of exceeding the limit is 67%, which is likely to pose a threat to the safety of human heart tissue. To obtain the degree of influence of relevant variables on the induced $E_{\max}$, the OMP-sgPCE and MC methods combined with the Sobol method are used for a global sensitivity analysis. The coil group's spatial location parameters have a considerable impact on the induced $E_{\max}$ in the human heart implanted with AVS, and the influence of the AVS geometric parameters cannot be ignored. This work can provide a reasonable theoretical basis and scientific guidance for design optimization of EV-WPT devices and AVS.

ACKNOWLEDGMENT

This work was supported in part by the Jilin Scientific and Technological Development Program under Grant 20230201122GX and Grant 20220101196JC, and in part by the Key Laboratory for Comprehensive Energy Saving of Cold Regions Architecture of Ministry of Education, Jilin Jianzhu University under Grant JLJZHDKF202203.

REFERENCES

1. Sim, B., S. Jeong, J. Kim, S. Park, S. Lee, S. Hong, J. Song, H. Kim, H. Kang, H. Park, D. Lho, and J. Kim, "A near field analytical model for EMI reduction and efficiency enhancement using an nth harmonic frequency shielding coil in a loosely coupled automotive WPT system," *IEEE Trans. Electromagn. Compat.*, Vol. 63, No. 3, 935–946, 2021.
2. Campi, T., S. Cruciani, F. Maradei, A. Andrea Montalto, F. Musumeci, and M. Feliziani, "EMI in a Cardiac Implantable Electronic Device (CIED) by the wireless powering of a Left Ventricular Assist Device (LVAD)," *IEEE Trans. Electromagn. Compat.*, Vol. 63, No. 4, 988–995, 2021.
3. Hong, S., T. Kim, S. Lee, S. Jeong, B. Sim, H. Kim, J. Song, S. Ahn, and J. Kim, "A frequency-selective EMI reduction method for tightly coupled wireless power transfer systems using resonant frequency control of a shielding coil in smartphone application," *IEEE Trans. Electromagn. Compat.*, Vol. 61, No. 6, 2031–2039, 2019.
4. Bosshard, R. and J. W. Kolar, "Multi-objective optimization of 50 kW/85 kHz IPT system for public transport," *IEEE J. Emerg. Sel. Top. Power Electron.*, Vol. 4, No. 4, 1370–1382, 2016.
5. Shin, J., S. Shin, Y. Kim, S. Ahn, S. Lee, G. Guho Jung, S. Jeon, and D. Cho, "Design and implementation of shaped magnetic-resonance-based wireless power transfer system for roadway-powered moving electric vehicles," *IEEE Trans. Ind. Electron.*, Vol. 61, No. 3, 1179–1192, 2014.
6. Choi, B., E. Kim, W. Shin, S. Park, and K. Kim, "Exposure assessment of a 20-kW wireless power transfer system for electric vehicles," *Int. J. Automot. Technol.*, Vol. 21, No. 6, 1349–1353, 2020.
7. Laakso, I. and A. Hirata, "Evaluation of the induced electric field and compliance procedure for a wireless power transfer system in an electrical vehicle," *Phys. Med. Biol.*, Vol. 58, No. 21, 7583–7593, 2013.
8. Budhia, M., J. T. Boys, G. A. Covic, and C. Y. Huang, "Development of a single-sided flux magnetic coupler for electric vehicle IPT charging systems," *IEEE Trans. Ind. Electron.*, Vol. 60, No. 1, 318–328, 2013.
9. Park, S., "Evaluation of electromagnetic exposure during 85 kHz wireless power transfer for electric vehicles," *IEEE Trans. Magn.*, Vol. 54, No. 1, 1–8, 2018.

10. Wang, Q., W. Li, J. Kang, and Y. Wang, "Electromagnetic safety evaluation and protection methods for a wireless charging system in an electric vehicle," *IEEE Trans. Electromagn. Compat.*, Vol. 61, No. 6, 1913–1925, 2019.
11. Bailey, W. H., R. Bodemann, J. Bushberg, C. K. Chou, R. Cleveland, A. Faraone, K. R. Foster, K. E. Gettman, K. Graf, T. Harrington, A. Hirata, R. R. Kavet, J. Keshvari, B. J. Klauenberg, A. Legros, D. P. Maxson, J. M. Osepchuk, J. P. Reilly, R. A. Tell, A. Thansandote, K. Yamazaki, M. C. Ziskin, and P. M. Zollman, "Synopsis of IEEE Std C95.1^{TM}— 2019 'IEEE standard for safety levels with respect to human exposure to electric, magnetic, and electromagnetic fields, 0 Hz to 300 GHz'," *IEEE Access*, Vol. 7, 171346–171356, 2019.
12. International Commission on Non-Ionizing Radiation Protection (ICNIRP): Gaps in Knowledge Relevant to the, "Guidelines for limiting exposure to time-varying electric and magnetic fields (1 Hz–100 kHz)," *Health Phys.*, Vol. 118, No. 5, 533–542, 2020.
13. Perpétuo, L., A. S. Barros, J. Dalsuco, R. Nogueira-Ferreira, P. Resende-Gonçalves, I. Falcão-Pires, R. Ferreira, A. Leite-Moreira, F. Trindade, and R. Vitorino, "Coronary artery disease and aortic valve stenosis: A urine proteomics study," *Int. J. Mol. Sci.*, Vol. 23, No. 21, 13579, 2022.
14. Kim, M., W. Lee, K. Kim, H. Lim, and Y. J. Kim, "A preclinical trial of perventricular pulmonary valve implantation: Pericardial versus aortic porcine valves mounted on self-expandable stent," *Artif. Organs.*, Vol. 45, No. 5, E89–E100, 2020.
15. Das, R. and H. Yoo, "RF heating study of a new medical implant lead for 1.5 T, 3 T, and 7 T MRI systems," *IEEE Trans. Electromagn. Compat.*, Vol. 59, No. 2, 360–366, 2017.
16. Shah, I. A., Y. Cho, and H. Yoo, "Safety evaluation of medical implants in the human body for a wireless power transfer system in an electric vehicle," *IEEE Trans. Electromagn. Compat.*, Vol. 63, No. 3, 681–691, 2021.
17. Shah, I. A. and H. Yoo, "Assessing human exposure with medical implants to electromagnetic fields from a wireless power transmission system in an electric vehicle," *IEEE Trans. Electromagn. Compat.*, Vol. 62, No. 2, 338–345, Apr. 2020.
18. Shah, I. A., A. Basir, Y. Cho, and H. Yoo, "Safety analysis of medical implants in the human head exposed to a wireless power transfer system," *IEEE Trans. Electromagn. Compat.*, Vol. 64, No. 3, 640–649, 2022.
19. Iqbal, A., M. Al-Hasan, I. B. Mabrouk, A. Basir, M. Nedil, and H. Yoo, "Biotelemetry and wireless powering of biomedical implants using a rectifier integrated self-diplexing implantable antenna," *IEEE Trans. Microw. Theory Tech.*, Vol. 69, No. 7, 3438–3451, 2021.
20. Wang, T., Y. Wu, B. Li, Q. Yu, L. Xu, and S. Guan, "Design of electric vehicle's wireless power transfer system based on deep learning combined with multi-objective optimization," *IEEE Trans. Compon. Pack. Manuf. Technol.*, Vol. 12, No. 12, 1983–1994, 2022.
21. Larbi, M., R. Trinchero, F. G. Canavero, P. Besnier, and M. Swaminathan, "Analysis of parameter variability in an integrated wireless power transfer system via partial least-squares regression," *IEEE Trans. Compon. Pack. Manuf. Technol.*, Vol. 10, No. 11, 1795–1802, 2020.
22. Yu, Q., J. Lin, X. Ma, B. Li, L. Xu, and T. Wang, "Efficiency optimization of wireless power transfer system for electric vehicle based on improved marine predators algorithm," *IEEE Trans. Intell. Transp. Syst.*, Vol. 24, No. 7, 7847–7858, 2023, doi: 10.1109/TITS.2022.3229958.
23. Wang, T., Q. Yu, B. Li, G. Lv, Y. Wu, and S. Guan, "Uncertainty quantification of human electromagnetic exposure from electric vehicle wireless power transfer system," *IEEE Trans. Intell. Transp. Syst.*, 1–11, 2023, doi: 10.1109/TITS.2023.3235807.
24. Cheng, X. and V. Monebhurrun, "Application of different methods to quantify uncertainty in specific absorption rate calculation using a CAD-based mobile phone model," *IEEE Trans. Electromagn. Compat.*, Vol. 59, No. 1, 14–23, 2017.
25. Sobol, I. M., "Global sensitivity indices for nonlinear mathematical models and their Monte Carlo estimates," *Math. Comput. Simul.*, Vol. 55, Nos. 1–3, 271–280, 2001.
26. Sudret, B., "Global sensitivity analysis using polynomial chaos expansions," *Reliab. Eng. Syst. Saf.*, Vol. 93, No. 7, 964–979, 2008.

27. Verma, M., J. Bassaganya-Riera, A. Leber, N. Tubau-Juni, S. Hoops, V. Abedi, X. Chen, and R. Hontecillas, "High-resolution computational modeling of immune responses in the gut," *GigaScience*, Vol. 8, No. 6, 2047–217X, 2019.
28. Kumar, D., A. Singh, P. Kumar, R. K. Jha, S. K. Sahoo, and V. Jha, "Sobol sensitivity analysis for risk assessment of uranium in groundwater," *Environ. Geochem. Health.*, Vol. 42, No. 6, 1789–1801, 2020.
29. Bdour, T. and A. Reineix, "Global sensitivity analysis and uncertainty quantification of radiated susceptibility in PCB using nonintrusive polynomial chaos expansions," *IEEE Trans. Electromagn. Compat.*, Vol. 58, No. 3, 939–942, 2016.
30. Barati, S., N. Fatouraee, M. Nabaei, L. Petrini, F. Migliavacca, G. Luraghi, and J. F. R. Matas, "Patient-specific multi-scale design optimization of transcatheter aortic valve stents," *Comput. Meth. Programs Biomed.*, Vol. 221, 106912–106925, 2017.
31. Christ, A., M. Douglas, J. Nadakuduti, and N. Kuster, "Assessing human exposure to electromagnetic fields from wireless power transmission systems," *Proc. IEEE*, Vol. 101, No. 6, 1482–1493, 2013.
32. International Commission on Non-Ionizing Radiation Protection (ICNIRP), "Guidelines for limiting exposure to time-varying electric and magnetic fields (1 Hz to 100 kHz)," *Health Phys.*, Vol. 99, No. 6, 818–836, 2010.
33. International Commission on Non-Ionizing Radiation Protection (ICNIRP), "Guidelines for limiting exposure to time-varying electric and magnetic fields (100 kHz to 300 GHz)," *Health Phys.*, Vol. 118, No. 5, 483–524, 2020.
34. Xiu, D. and G. E. Karniadakis, "The Wiener-Askey polynomial chaos for stochastic differential equations," *SIAM J. Sci. Comput.*, Vol. 22, No. 2, 619–644, 2002.